Ethanol-to-Olefins conversion using CeO_2 and In_2O_3 modified Beta zeolites in a stacked-bed reactor system

Roberta de Souza Costa[1]*, Raquel Massad Cavalcante[1], Mônica Antunes Pereira da Silva[1]

[1] *Escola de Química, Universidade Federal do Rio de Janeiro, Rio de Janeiro, Brazil, 21949-900.*
**e-mail: rcosta@eq.ufrj.br*

Resumo/Abstract

RESUMO - Catalisadores baseados na zeólita Beta modificada com CeO_2 e In_2O_3 foram preparados por precipitação por deposição e empregados na conversão de etanol em olefinas. As amostras foram caracterizadas por espectrometria de emissão óptica com plasma acoplado indutivamente (ICP-OES), difração de raios X (DRX), espectroscopia de ressonância magnética nuclear com rotação no ângulo mágico (RMN-MAS) de ^{29}Si e ^{27}Al, fisissorção de nitrogênio, além de dessorção à temperatura programada de amônia e dióxido de carbono (TPD-NH_3 e TPD-CO_2). Diferentes composições e configurações de leito catalítico, incluindo leitos simples e em série contendo In_2O_3 ou CeO_2 e zeólita Beta, foram investigadas a 475 °C. Os óxidos CeO_2 e In_2O_3 apresentaram maior concentração de sítios básicos, enquanto os catalisadores CeO_2/Beta e In_2O_3/Beta demonstraram acidez característica da interação entre a zeólita e os óxidos metálicos. Dentre os sistemas avaliados, o sistema de leito em série contendo In_2O_3 sobre a zeólita Beta apresentou maior resistência à formação de coque e favoreceu a formação de propeno pela rota de desidrogenação do etanol.
Palavras-chave: zeólita Beta, óxidos metálicos, etanol, propeno, olefinas.

ABSTRACT - Beta zeolite-based catalysts modified with CeO_2 and In_2O_3 were prepared via deposition-precipitation and employed in the conversion of ethanol to olefins. The samples were characterized by inductively coupled plasma optical emission spectrometry (ICP-OES), X-ray diffraction (XRD), magic-angle spinning nuclear magnetic resonance (MAS NMR) of ^{29}Si and ^{27}Al, nitrogen physisorption, and temperature-programmed desorption of ammonia and carbon dioxide (TPD-NH_3 and TPD-CO_2). Different catalyst compositions and reactor bed configurations, including both single- and dual-layer arrangements of In_2O_3 or CeO_2 and Beta zeolite, were investigated at 475 °C. The CeO_2 and In_2O_3 oxides exhibited a higher concentration of basic sites, while the CeO_2/Beta and In_2O_3/Beta catalysts showed acidity characteristic of the interaction between the zeolite and metal oxides. Among the tested systems, the stacked-bed reactor system containing In_2O_3 over Beta zeolite demonstrated greater resistance to coke formation and promoted propylene formation via the ethanol dehydrogenation pathway.
Keywords: Zeolite Beta, metal oxides, ethanol, propylene, olefins.

Introduction

In Brazil, the implementation of the National Biofuels Policy (RenovaBio) was primarily designed to support the country's commitments under the Paris Agreement by promoting a greater share of biofuels in the national energy matrix. Under this policy, fuel distributors must meet individual decarbonization targets by purchasing Decarbonization Credits (CBIOs) (1). One effective strategy to achieve these targets involves producing chemicals traditionally derived from petrochemical routes using ethanol—a renewable and widely available resource in the country.

While ethanol is widely used as a fuel, its potential as a chemical intermediary feedstock is also significant. However, expanding its use in the chemical industry poses challenges, particularly regarding the development of high-performance catalysts and cost reduction, which are necessary to make biomass-derived routes competitive with established fossil-based processes. Therefore, the conversion of ethanol into value-added chemicals may become economically viable (2–4).

Ethanol is a versatile platform molecule for the synthesis of key petrochemical compounds, including ethylene, 1,3-butadiene, propylene, and higher hydrocarbons (5–7). However, the production costs of these compounds via ethanol-derived routes is still economically less competitive to conventional fossil-based processes (8).

The production of olefins from ethanol has attracted increasing attention as it offers a more sustainable alternative to traditional petrochemical routes, which are associated with generating of a wide range of pollutants and the need for environmental treatment units (3,9). For instance, catalytic cracking processes emit greenhouse gases such as CO, CO_2, NOx, and particulate matter from coke combustion in the regenerator (3). This environmental impact underscores the need for alternative pathways, such as ethanol-to-olefins conversion, which can substantially reduce emissions associated with conventional petrochemical production.

The ethanol dehydrogenation route enables the formation of several hydrocarbons of high commercial value, with

metal oxide-based catalysts being the most employed in this process. The main target compound is 1,3-butadiene (10–12), although more recent studies have also reported the formation of propylene (5,6,13–15).

Metal oxide catalysts promote the formation of propylene and isobutene with high selectivity, producing lower amounts of coke compared to dehydration-based processes. In this route, ethanol is initially dehydrogenated to acetaldehyde, which is subsequently converted into ketones. These intermediates then undergo further chemical transformations to yield C3 and C4 olefins. The literature generally agrees that the dehydrogenation catalyzed by basic sites, followed by aldol condensation reactions, plays a key role in this process (6,14,16–18).

Recent studies on ethanol conversion have shown that metal oxides, such as CeO_2 and In_2O_3, either used alone or in combination with zeolites, enable the formation of C3 and C4 olefins through reaction pathways that differ from those traditionally described using zeolites (5,14,15,19).

In this context, the present study aims to investigate ethanol conversion using zeolites and metal oxides, focusing on evaluating the product distribution resulting from dehydration and dehydrogenation pathways.

Experimental

Catalyst preparation

The In_2O_3/Beta and CeO_2/Beta catalysts were prepared according to the deposition precipitation method described by Xue *et al.* (2017) (15). Fifteen grams of Beta zeolite (CENPES – PETROBRAS) were dispersed in 250 mL of NH_4OH solution (3 mol L^{-1}), previously adjusted to pH 9. For the In_2O_3-containing catalysts, a 0.9 mol L^{-1} solution of $In(NO_3)_3$ was prepared, while for the CeO_2-containing catalysts, a 0.6 mol L^{-1} solution of $(NH_4)_2Ce(NO_3)_6$ was used. The precursor salt solution was added dropwise to the Beta suspension, under continuous stirring, and at room temperature. Simultaneously, a 3 mol L^{-1} NH_4OH solution was added dropwise to maintain the pH at 9 throughout the addition of the precursor solution. The volumes of the solutions were calculated to yield a final oxide loading of 40 wt% (In_2O_3 or CeO_2) relative to the support. The resulting solids were filtered, dried for 12 hours, and calcined under a flow of synthetic air at 500°C for 5 hours. The same procedure was used to prepare the pure oxides, except the precursor solutions were added dropwise into a beaker containing 250 mL of 3 mol L^{-1} NH_4OH solution adjusted to pH 9.

Catalyst characterization

Magic angle nuclear magnetic resonance (NMR-MAS) spectroscopy for ^{29}Si and ^{27}Al was conducted using a Bruker Avance III 400 instrument operating at 9.4 Tesla. Inductively coupled plasma optical emission spectrometer (ICP-OES) measurements were conducted using a Horiba Scientific Ultima 2 instrument. Physisorption analysis was carried out using the ASAP 2020 Plus system, employing N_2 adsorption at - 196 ºC after sample pretreatment at 300 °C under vacuum for 18 h. X-ray diffraction (XRD) patterns were obtained using a Rigaku Miniflex diffractometer with CuKα radiation (λ = 1.5417 Å, 30 kV, 15 mA, scan rate 0.05 °/s).

The catalysts' acidity and basicity were determined by temperature-programmed desorption of ammonia (TPD-NH_3) and carbon dioxide (TPD-CO_2), respectively. These analyses were performed using a multipurpose analytical system coupled with a PFEIFFER QMG-220 mass spectrometer.

In the TPD-NH_3 experiments, a 4% NH_3/He gas mixture was passed over the sample at 70 ºC for 30 minutes at a flow rate of 30 mL min^{-1}. Desorption was carried out from 70 to 1000°C at a heating rate of 20 ºC min^{-1}, using a 30 mL min^{-1} He flow, while monitoring the m/z=15 fragment. For TPD-CO_2, the sample was exposed to 10% CO_2/He mixture at room temperature (30 mL min^{-1}). Desorption was conducted from 30 to 1000 °C at 20 ºC min^{-1} and a He flow rate of 30 mL min^{-1}, while monitoring the m/z=44 fragment.

Catalytic tests

Catalytic reactions were conducted in a fixed-bed tubular reactor operating at atmospheric pressure, using 0,4 g of catalyst. In_2O_3-based catalysts were pretreated *in situ* under N_2 flow (30 mL min^{-1}) at 500 ºC (heating rate: 10 ºC min^{-1}) for 1 h. CeO_2-based catalysts were pretreated in three steps: (1) dried at 150 ºC under N_2 flow (50 mL min^{-1}) for 30 min; (2) reduced under 10 % H_2/N_2 flow (100 mL min^{-1}) at 500 ºC for 1 hour, and (3) oxidized under synthetic air (30 mL min^{-1}) at 500 ºC for 30 min. The distinct pretreatments for CeO_2 and In_2O_3 based catalysts were adopted due to the known loss of surface area caused by sintering during indium reduction, even when followed by subsequent reoxidation (20). Ethanol was introduced using a syringe pump and vaporized at 200 ºC, with a carrier N_2 flow of 22 mL min^{-1}.

Additional tests were performed using dual-layer (stacked bed) configurations to assess the influence of catalyst arrangement and the effect of molecular migration on catalytic performance. In these experiments, 0.16 g of either CeO_2 or In_2O_3 and 0.24 g of Beta zeolite were used to maintain a 40 wt% oxide loading in the total catalyst bed. A thin layer of quartz wool was inserted between the two materials to prevent direct contact and create distinct reaction zones.

The notation CeO_2||Beta denotes the configuration with CeO_2 at the top of the bed, exposed first to the gas stream under downward flow conditions. Conversely, Beta||CeO_2 indicates Beta zeolite at the top. The same notation applies to In_2O_3||Beta and Beta||In_2O_3 configurations. The reactions were conducted at 475 ºC, keeping the weight hourly space velocity (WHSV) constant at 4.7 $g_{ethanol}$ $g_{catalyst}$ h^{-1}. The reactor effluent was analyzed by CG Agilent 6890 with an

HP-PLOT/Q capillary column and a flame ionization detector.

The product yield (Yi), instantaneous productivity (IPi), and cumulative productivity (CPi) of product i were calculated according to Equations 1 to 3:

$$Y_i = \frac{\text{mass of ethanol consumed to form the product i}}{\text{mass of ethanol fed}} \quad (1)$$

$$IP_i = Y_i \times WHSV \times F \times (M_i/M_e) \quad (2)$$

$$CPi = \int_0^{t_n} (IP_i)\ dt \quad (3)$$

where: WHSV represents the weight hourly space velocity ($g_{ethanol}\ g_{catalyst}\ h^{-1}$), F is the stoichiometric molar ratio of product i to ethanol, Mi and Me are the molar masses of product i and ethanol, respectively and t_n is the sampling time.

Results and discussion

Catalyst characterization

Table 1 presents the composition determined by ICP-OES for the oxides (CeO_2 and In_2O_3) incorporated into the CeO_2/Beta and In_2O_3/Beta catalysts. It also includes the framework SiO_2/Al_2O_3 ratio (SAR) obtained by ^{29}Si NMR analysis, and the amount of extra-framework aluminum (Al_{extra}) determined by ^{27}Al NMR analysis. The oxide contents incorporated into the Beta zeolite were found to be very close to the nominal values, indicating that the precipitation-deposition preparation method was efficient.

However, a decrease in the framework SAR is noted for the CeO_2/Beta and In_2O_3/Beta catalysts, which can be attributed to a desilication process. Dos Santos *et al.* (21) reported a similar phenomenon when treating Beta zeolite in an alkaline medium to generate mesopores, noting a reduction in the amount of Si(0Al) and the framework SAR due to desilication. Considering that the preparation of the CeO_2/Beta and In_2O_3/Beta catalysts was carried out under alkaline conditions (pH 9), it is plausible that a similar desilication process occurred.

Table 1. Oxide composition, framework SAR, and extra-framework aluminum content.

Catalyst	Oxide (%)[a]	SAR [b]	Al_{extra} (%)[c]
Beta	0	30.6	31.1
CeO_2/Beta	39.9	14.4	26.7
In_2O_3/Beta	41.1	19.9	13.8
CeO_2	n.e.	n.e.	n.e.
In_2O_3	n.e.	n.e.	n.e.

[a]-ICP-OES analysis; [b] -RMN^{29}Si analysis; [c]-RMN^{27}Al analysis; n.e. – not evaluated.

Additionally, a slight decrease in the percentage of Al_{extra} is observed in the CeO_2/Beta and In_2O_3/Beta catalysts, suggesting that the oxide incorporation method did not lead to significant dealumination of the Beta zeolite.

The X-ray diffraction (XRD) patterns are shown in Figure 1. Figure 1(a) presents the Beta, CeO_2, and CeO_2/Beta catalysts, allowing for a comparison of the effects of CeO_2 incorporation on the crystalline structure of the Beta zeolite. Similarly, Figure 1(b) displays the XRD patterns of the Beta, In_2O_3, and In_2O_3/Beta catalysts, enabling an evaluation of the structural modifications induced by incorporating of In_2O_3 into the Beta zeolite.

Figure 1. XRD patterns of Beta, CeO_2, and CeO_2/Beta (a) and Beta, In_3O_2, and In_3O_2/Beta (b) catalysts.

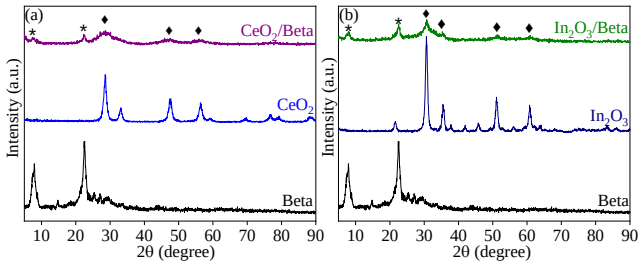

Figure 1(a) shows that the diffractogram of CeO_2 exhibits characteristic peaks at 28.6°, 33.1°, 47.6°, and 56.3°, consistent with the JCPDS database 43-1002 and as previously reported in the literature (22), with the most intense reflection at 28.6°. Similarly, Figure 1(b) presents the characteristic diffraction peaks of In_2O_3 at 21.5°, 30.6°, 35.5°, 51.1°, and 60.7°, corresponding to the PDF# 06-0416 (15), with the main diffraction peak observed at 30.6°. For the CeO_2/Beta and In_2O_3/Beta catalysts, the diffractograms reveal the presence of reflections associated with both the Beta zeolite (7.85° and 22.50°), according to ICDD 42-0024 (23) and the respective metal oxides. Nevertheless, the incorporation of a significant amount of oxide into the Beta zeolite framework resulted in a decrease in the intensity and a broadening of the Beta-related peaks. According to Shi *et al.*(22), the reduction in peak intensity is attributed to the coverage of zeolite crystals by the metal oxides due to the deposition–precipitation process. On the other hand, the broadening of the diffraction peaks has been associated with a decrease in crystallite size, as reported by Xue *et al.* (15).

Table 2 presents the textural properties, total acid site density, and total basic site density of the Beta, CeO_2/Beta, In_2O_3/Beta, CeO_2, and In_2O_3 catalysts.

Table 2. Textural properties, total acid site density, and total basic site density of the catalyst.

Catalyst	Specific area ($m^2\ g^{-1}$)[a]	Micro pore vol. ($cm^3\ g^{-1}$)[b]	Total acid sites (µmol g_{cat}^{-1})	Total basic sites (µmol g_{cat}^{-1})
Beta	485	0.15	2418	37
CeO_2/Beta	348	0.07	1576	32
In_2O_3/Beta	309	0.08	1688	39
CeO_2	58	0.001	186	243
In_2O_3	69	0.003	283	93

[a] BET method; [b] t-plot method

A significant decrease in specific area and micropore volume was observed for the CeO_2/Beta and In_2O_3/Beta catalysts, which can be attributed to the partial blockage of the zeolite's micropores by the incorporated oxides

(6,15,24). CeO_2 and In_2O_3 nanoparticle oxides also exhibited low specific areas and negligible micropore volumes (15).

The Beta catalyst exhibited the highest total acidity, whereas CeO_2 and In_2O_3 oxides showed significantly lower acid site densities. Similar findings were reported by Jin *et al.* (14,24), who observed a reduced number of acid sites on CeO_2 through NH_3-TPD analysis. Furthermore, Xue *et al.* (6,15) demonstrated that In_2O_3, in addition to its low total acidity, lacks Brønsted acid sites, as evidenced by its inactivity in the cumene cracking reaction, an indicator of Brønsted acidity. Accordingly, the acidity profiles of the CeO_2/Beta and In_2O_3/Beta catalysts result from the combination of the Beta zeolite and the respective incorporated oxides (6,14,15,24). As expected, incorporating metal oxides into Beta zeolite reduced the total number of acid sites.

The Beta, CeO_2/Beta, and In_2O_3/Beta catalysts exhibited similar total basic site densities, indicating that the deposition–precipitation method used to incorporate CeO_2 and In_2O_3 did not significantly alter the basicity of the zeolite. These findings are consistent with those of Jin *et al.* (14), who reported comparable total basic site densities for pure Beta zeolite and YCe/Beta composites. Similarly, Xue *et al.* (15) showed that for In_2O_3/Beta composites containing 30%, 40%, and 50% In_2O_3, maintained basicity levels similar to those of the pure Beta zeolite. In contrast, CeO_2 and In_2O_3 catalysts alone exhibited the highest total basic site densities, with CeO_2 displaying the most significant number of basic sites among the evaluated catalysts.

Catalytic test

All catalysts achieved complete ethanol conversion. However, product distribution varied with reaction time.

Figures 2 and 3 present the product distribution from ethanol conversion after 15 and 157 minutes of reaction, respectively, for catalysts containing CeO_2 and In_2O_3. The data are presented as a function of bed configuration and composition at 475 °C and a weight hourly space velocity (WHSV) of 4.7 $g_{ethanol}\, g_{catalyst}\, h^{-1}$. Reaction products included C1 to C3 paraffins (C1-C3 par), ethylene (C2=), propylene (C3=), C4 hydrocarbons (C4's), diethyl ether (DEE), acetaldehyde (C_2H_4O), acetone, isopropanol, C5 hydrocarbons (C5's), and heavier hydrocarbons with six or more carbon atoms (C6+).

As shown in Figure 2, the reactor operated with the Beta||CeO_2 exhibited behavior similar to that of the CeO_2/Beta catalyst, characterized by the predominance of ethylene formation after 157 minutes of reaction. These results suggest that, in these configurations, ethanol dehydration was the main reaction pathway, accompanied by a loss of catalytic stability likely due to coke formation (14).

The CeO_2||Beta configuration, although producing C_1–C_3 paraffins (~30%) within the first 15 minutes of reaction, exhibited the lowest degree of deactivation of the actives sites responsible for propylene and higher hydrocarbon formation (23) among the systems containing Beta zeolite after 157 minutes. Under these conditions, the main products were propylene, C_1–C_3 paraffins, and C_4 hydrocarbons, each with yields of 10%. Notably, the only system in which products from the dehydrogenation pathway were observed consisted exclusively of CeO_2.

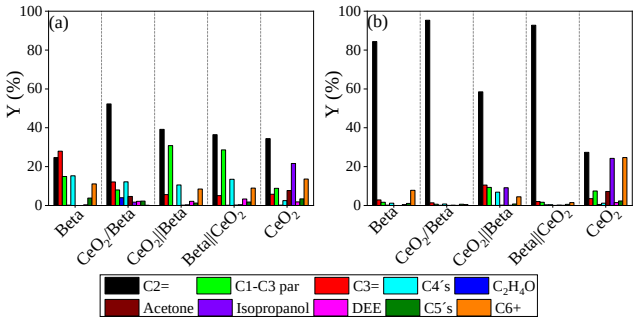

Figure 2. Product distribution from ethanol conversion after 15 (a) and 157 min (b) of reaction for catalysts containing CeO_2 as a function of bed configuration and composition, at 475 °C and a WHSV of 4.7 $g_{ethanol}\, g_{catalyst}\, h^{-1}$.

During the first 15 minutes of reaction, the In_2O_3||Beta configuration exhibited high yield toward C_1–C_3 paraffins (40%) and a moderate formation of C_4 and C_6+ hydrocarbons (~20%).

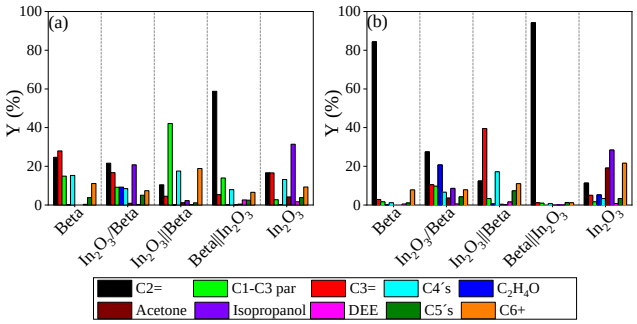

Figure 3. Product distribution from ethanol conversion after 15 (a) and 157 min (b) of reaction for catalysts containing In_2O_3, as a function of bed configuration and composition, at 475 °C and a WHSV of 4.7 $g_{ethanol}\, g_{catalyst}\, h^{-1}$.

No products resulting from ethanol dehydrogenation were observed during this initial period. However, after 157 minutes of reaction, propylene yielded approximately 40%, while C_4 hydrocarbon formation remained around 20%.

On the other hand, the Beta||In_2O_3 system showed, after 157 minutes of reaction, behavior similar to that of isolated Beta zeolite, suggesting that the dehydration pathway was predominant. This result indicates coke deposition, which likely deactivated the catalytic sites responsible for the formation of higher hydrocarbons. For the system containing only In_2O_3, propylene formation was observed within the first 15 minutes of the reaction. However, after 157 minutes, the major products originated from the dehydrogenation pathway.

Figure 4 shows the instantaneous productivity of ethylene (IPE) and propylene (IPP) as a function of reaction time at 475 °C, for the In_2O_3/Beta, In_2O_3||Beta, CeO_2/Beta, CeO_2||Beta, and Beta systems.

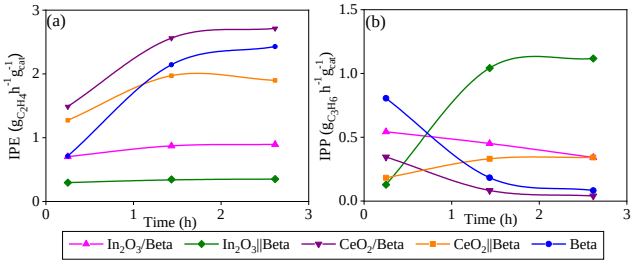

Figure 4. Instantaneous productivity of ethylene (a) and propylene (b) for In_2O_3/Beta, In_2O_3||Beta, CeO_2/Beta, CeO_2||Beta, and Beta systems, as a function of reaction time, at 475 °C and a WHSV of 4.7 $g_{ethanol}$ $g_{catalyst}$ h^{-1}.

The Beta catalyst showed a progressive increase in IPE and a simultaneous decline in IPP as a function of rection time, suggesting the deactivation of active sites likely due to coke deposition. In contrast, CeO_2/Beta and In_2O_3/Beta exhibited higher IPE, while the systems CeO_2||Beta and In_2O_3||Beta showed increased IPP and greater resistance to deactivation, especially the In_2O_3||Beta system. These results highlight the interaction between basic sites (CeO_2 or In_2O_3) and acidic sites (Beta) is essential for propylene production via dehydrogenation (24).

Table 3 presents the cumulative productivities of the main products obtained over the individual catalysts (Beta, CeO_2, In_2O_3, CeO_2/Beta, and In_2O_3/Beta), as well as the stacked bed configurations (CeO_2||Beta and In_2O_3||Beta) after 157 minutes of reaction at 475 °C.

Table 3. Cumulative productivity of products from ethanol conversion after 157 minutes of reaction at 475 °C.

Cat.	Cumulative productivity g g_{cat}^{-1}					
	C_2H_4	C_3H_6	C1-C3 par	C4's	Acetone	Isopropanol
Beta	5.5	0.7	0.4	0.4	n.e.	n.e.
CeO_2	2.3	0.3	0.7	0.1	0.8	1.2
CeO_2/Beta	5.9	0.4	0.2	0.4	0.3	0.2
CeO_2||Beta	4.5	0.7	1.5	0.7	0.1	0.3
In_2O_3	1.0	0.8	0.2	0.6	1.0	3.1
In_2O_3/Beta	2.1	1.2	0.9	0.6	0.3	1.7
In_2O_3||Beta	0.9	2.0	1.4	1.2	0.1	0.1

n.e. – not evaluated

The analysis of cumulative productivities for CeO_2 and In_2O_3 reveals that the ethanol dehydrogenation pathway was predominant. However, detecting products associated with the dehydration route indicates that both reaction pathways occurred within these catalytic systems.

For the CeO_2 catalyst, significant amounts of isopropanol and acetone were observed, confirming the dominance of the dehydrogenation route. Nonetheless, small quantities of ethylene, propylene, and C1–C3 paraffins were also detected. According to Table 2, the low concentration of total acid sites may be associated with the formation of these light hydrocarbons, suggesting that even limited acidity in the catalytic system can promote dehydration reactions and carbon chain growth.

A similar behavior was observed for the In_2O_3 catalyst, although with an even more substantial predominance of the dehydrogenation pathway. The cumulative productivity of isopropanol reached approximately 3.1 g g_{cat}^{-1}, nearly three times higher than that obtained with CeO_2 (1.2 g g_{cat}^{-1}). According to Jin *et al.*(14), the conversion of acetone to isopropanol and, subsequently, to propylene is promoted by acid sites. As shown in Table 2, In_2O_3 exhibits a total acidity of 283 µmol g_{cat}^{-1}, compared to 186 µmol g_{cat}^{-1} for CeO_2.

Although products derived from dehydration were also identified, the cumulative productivity values for propylene suggest that it was primarily formed via the dehydration of isopropanol, consistent with the mechanism proposed by Jin *et al*. (14).

In the evaluation of the CeO_2||Beta stacked bed system, higher yields of propylene and C1–C3 paraffins were observed compared to the CeO_2/Beta catalyst, accompanied by a slight increase in isopropanol formation. These results suggest that the CeO_2||Beta configuration promoted the formation of propylene from isopropanol derived from the ethanol dehydrogenation pathway, whereas the CeO_2/Beta catalyst predominantly favored the ethanol dehydration route.

This behavior is attributed to the sequential structure of the stacked bed, in which ethanol first contacts the CeO_2 layer, facilitating its transformation into acetone and subsequently into isopropanol. Upon reaching the acidic surface of Beta zeolite, isopropanol undergoes dehydration, leading to the formation of propylene.

The In_2O_3/Beta catalyst demonstrated high efficiency in propylene production. The significant formation of acetaldehyde and isopropanol, combined with low ethylene yields, suggests that propylene was predominantly produced via the dehydrogenation pathway. The synergy between In_2O_3 and the Beta zeolite appears to have favored this route by integrating both basic and acidic active sites.

Ethanol is initially converted into acetone over In_2O_3, which then diffuses to the Beta zeolite. There, acetone undergoes a *Meerwein–Ponndorf–Verley* (MPV) reduction by unreacted ethanol to form isopropanol, dehydrated to yield propylene (5,6,14,15,24). The short diffusion path between the two components in the bifunctional catalyst facilitates this sequence of transformations.

The In_2O_3||Beta stacked bed system proved even more effective in promoting propylene formation compared to the In_2O_3/Beta catalyst. In addition to propylene, C1–C3 paraffins, C4 hydrocarbons, and minor amounts of ethylene were detected. The low concentrations of acetone and isopropanol suggest that the dehydrogenation pathway proposed by Jin *et al.* (14) and Xia *et al.* (19) was predominant, leading to the near-complete conversion of isopropanol (derived from acetone) into propylene.

Furthermore, the small quantities of ethylene and the presence of C1–C3 paraffins and C4 hydrocarbons indicate that the dehydration route was also active, albeit to a lesser extent. This secondary activity can be attributed to the moderate acidity of both In_2O_3 and Beta zeolite.

Conclusions

Catalysts based on Beta zeolite modified with CeO_2 and In_2O_3 exhibited distinct structural and acid–base properties resulting from the interaction between the zeolite and the metal oxides. The observed reductions in specific area, microporosity, and XRD peak intensities suggest partial surface coverage of the zeolite by oxide particles. The incorporation of CeO_2 and In_2O_3 led to a reduction in density of acid sites relative to pure Beta zeolite, while strong acid sites were retained, particularly in the CeO_2-modified samples Although CO_2 temperature desorption revealed no significant changes in surface density for the impregnated materials, the pure oxides exhibited a greater density of basic sites, with CeO_2 being the most basic. Dual-layer catalytic systems (CeO_2||Beta and In_2O_3||Beta) showed enhanced performance in terms of stability and propylene selectivity due to the promotion of the ethanol dehydrogenation pathway. The proposed mechanism involves the sequential conversion of ethanol to acetaldehyde, then to acetone, followed by hydrogenation to isopropanol and subsequent dehydration to propylene. Among the stacked-bed reactor configurations evaluated, In_2O_3||Beta emerged as the most promising, system, showing high selectivity toward propylene and strong resistance to deactivation. These findings highlight a positive synergy between acid and base functions, which is essential to promote the desired steps in converting ethanol to light olefins.

Acknowledgments

Mônica A. P. da Silva acknowledges the financial support received from CNPq (Conselho Nacional de Desenvolvimento Científico e Tecnológico) Grant number 307190/2022-6 and FAPERJ (Fundação Carlos Chagas Filho de Amparo à Pesquisa do Estado do Rio de Janeiro) Grant number E-26/211.578/2021. The authors also thank Laboratório Multiusuário RMN de sólidos (LABRMN1/IQ/UFRJ), Laboratório de Tecnologia do Hidrogênio (LABTECH/EQ/UFRJ), Centro de Tecnologia Mineral (CETEM/MCTI)for characterization analyses.

References

1. ANP, RenovaBio, *gov.br*, 2024. https://www.gov.br/anp/pt-br/canais_atendimento/imprensa/noticias-comunicados/renovabio-anp-publica-metas-preliminares-de-reducao-de-emissoes-de-gases-causadores-de-efeito-estufa-para-2025 (accessed Jan. 15, 2025).
2. J. M. R. Gallo; J. M. C. Bueno; U. Schuchardt, *J. Braz. Chem. Soc.* **2014,** *25*, 12, 2229–2243.
3. M. H. Morad, *Arab. J. Chem.*, **2024,** *17*, 105560, 2024.
4. I. M. S. Anekwe; Y. M. Isa, *Int. J. Energy Res.* **2023,** *2023*, 1–28.
5. C. R. V. Matheus; L. H. Chagas; G. G. Gonzalez; E. S. Falabella Aguiar; L. G. Appel, *ACS Catal.* **2018,** *8*, 7667–7678.
6. F. Xue; C. Miao; Y. Yue; W. Hua; Z. Gao, *Fuel Process. Technol.*, **2019,** *186*, 110–115.
7. Y. Fan; W. Xia; C. Ma; Y. Huang; S. Li; X. Wang; C. Qian; K. Chen; D. Liu, *Chem. Eng. Sci.*, **2023,** *270*, 118532.
8. C. Angelici; B. M. Weckhuysen; P. C. A. Bruijnincx, *ChemSusChem*, **2013,** *6*, 1595–1614.
9. Q. A. Domingues; C. N. Passos; D. F. da S. Lage; E. C. Sousa; M. A. Araújo, *Processamento de Petróleo e Gás*, Petrobrás, Rio de Janeiro, 2014.
10. V. L. Sushkevich; I. I. Ivanova, *Appl. Catal. B Environ.* **2017,** *215*, 36–49.
11. M. Iwamoto, *Catal. Today* **2015,** *242*, 243–248.
12. V. L. Sushkevich; D. Palagin; I. I. Ivanova, *ACS Catal.* **2015,** *5*, 4833–4836.
13. S. M. Jin; K.-Y. Lee; D.-W. Lee, *J. Ind. Eng. Chem.* **2022,** *112*, 296–306.
14. H. Jin; Y. Yue; C. Miao; C. Tian; W. Hua; Z. Gao, *Catal. Letters*, **2023,** *153*, 230–238.
15. F. Xue; C. Miao; Y. Yue; W. Hua; Z. Gao, *Green Chem.* **2017,** *19*, 5582–5590.
16. H. M. Gobara; W. A. Aboutaleb; K. M. Hashem; S. A. Hassan; S. A. Henein, *J. Mater. Sci.* **2017,** *52*, 550–568.
17. M. Iwamoto; S. Mizuno; M. Tanaka, *Chem. a Eur. J.* **2013,** *19*, 7214–7220.
18. J. Sun; Y. Wang, *ACS Catal.* **2014,** *4*, 1078–1090.
19. W. Xia; F. Wang; L. Wang; J. Wang; K. Chen, *Catal. Commun.* **2017,** *90*, 10–13.
20. P.C. Zonetti; V.L. Bridi; G.G. Gonzalez; C.R. Moreira, O.C. Alves; R.R. de Avillez; L.G. Apple, *Chem Cat Chem*, **2019**, *11*, 4011-1020.
21. L. R. M. Dos Santos; M. A. P. Da Silva; S. C. De Menezes; L. S. Chinelatto; Y. L. Lam, *Micropor. Mesopor. Mat.* **2016,** *226*, 260–266.
22. Y. Shi; X. Wang; Y. Xia; C. Sun; C. Zhao; S. Li; W. Li, *Mol. Catal.* **2017,** *433*, 265–273.
23. A. Astafan; M.A. Benghalem; Y. Pouilloux; J. Patarin; N. Bats; C. Bouchy; T.J. Daou; L. Pinard *J. Catal.* **2016,** *336*, 1–10.
24. H. Jin; C. Miao; Y. Yue; C. Tian; W. Hua; Z. Gao, *Catal.* **2022,** *12*, 407.